Technical Note: ~~Oxygen Optodes on Profiling Platforms:~~ Update on ~~Response Times~~response times, ~~In-Air Measurements~~in-air measurements, and ~~In-Situ Drift~~in-situ drift for oxygen optodes on profiling platforms.

Henry C. Bittig[1] and Arne Körtzinger[2,3]

[1]Sorbonne Universités, UPMC Université Paris 06, CNRS, UMR 7093, Laboratoire d'Océanographie de Villefranche (LOV), Villefranche-sur-Mer, France
[2]GEOMAR Helmholtz-Zentrum für Ozeanforschung Kiel, Kiel, Germany
[3]Christian-Albrechts-Universität zu Kiel, Kiel, Germany

Correspondence to: Henry Bittig (bittig@obs-vlfr.fr)

Abstract. Oxygen optode measurements on floats and gliders suffer from a slow time response and ~~sensors that are or eventually run out of calibration~~various sources of drift in the calibration coefficients. Based on two dual-O_2 Argo floats, we show how to post-correct for the effect of the optode's time response and give an update on optode in-situ drift stability and in-air calibration. Both floats are equipped with an unpumped Aanderaa 4330 optode and a pumped Sea-Bird SBE63 op-
5 tode. Response times for the pumped SBE63 were derived after Bittig et al. (2014)~~. Also their~~ and the same methods were used to correct the time response bias. Using both optodes on each float, the time response regime of the unpumped Aanderaa optode was characterized more accurately than previously possible. Response times for the pumped SBE63 on profiling floats are in the range of $25 - 40$ s, while they are between $60 - 95$ s for the unpumped 4330 optode. Our parameterization can be employed to post-correct the slow optode time response on floats and gliders. After correction, both sensors agree to
10 within $2 - 3$ µmol kg^{-1} (median difference) in the strongest gradients (120 µmol kg^{-1} change over 8 minutes or 20 dbar) and better elsewhere. However, time response correction is only possible if measurement times are known, i.e., provided by the platform as well as transmitted and stored with the data. The O_2 in-air measurements show a significant in-situ optode drift of ~~−0.4~~−0.40 % yr^{-1} and ~~−0.2~~−0.27 % yr^{-1} over the available 2 and 3 years of deployment, respectively. Optode in-air measurements are systematically biased high during mid-day surfacings compared to dusk, dawn, and nighttime. While
15 preference can be given to nighttime surfacings to avoid this in-air calibration bias, we suggest a parameterization of the daytime effect as function of the sun's elevation to be able to use all data and to better constrain the result. Taking all effects into account, calibration factors have an uncertainty of 0.1 %. In addition, in-air calibration factors vary by $0.1 - 0.2$ % when using different reanalysis models as reference. The overall accuracy that can be achieved following the proposed correction routines is ~~< 1~~better than 1 µmol kg^{-1}.

1 Introduction

While oceanic oxygen measurements of the last century were mostly based on Winkler titrations of discrete water samples or profiles acquired with CTD-mounted electrochemical oxygen sensors, ~~they~~ such observations rely increasingly on O_2 optode sensors (Tengberg et al., 2006) deployed on autonomous platforms~~: The~~. In particular, the planning for a global Biogeochemical-Argo observation network of profiling floats equipped with biogeochemical sensors (including O_2 optodes) is well underway (Johnson and Claustre, 2016) ~~. Also,~~ and the use of gliders is becoming more operational (e.g., EGO: Testor et al., 2012).

Apart from cost effectiveness, the main reasons for this are improved sensor performance and characterization with respect to temperature and O_2 response (e.g., Bittig et al., 2012), hydrostatic pressure (Uchida et al., 2008; Bittig et al., 2015a), time response (Bittig et al., 2014), and O_2 drift behaviour (D'Asaro and McNeil, 2013; Bittig and Körtzinger, 2015; Bushinsky et al., 2016) as well as improved accuracy, either through in-air measurements during deployment or careful pre-/post-deployment calibrations for short deployments, e.g., of gliders.

It is therefore timely and useful to revisit the foundations of both pumped and unpumped O_2 optode behaviour on autonomous, profiling platforms, to ensure optimal data post-processing and best data quality. In this technical note, we want to refine the findings of Bittig et al. (2014) on the optode time response and of Bittig and Körtzinger (2015) on in-air measurements and in-situ drift stability.

2 Instrument Description

This study utilizes data from two dual-O_2 Navis floats (Sea-Bird Inc., Bellevue, USA) with WMO ID 6900889 and 6900890 that were deployed in the Eastern Tropical North Atlantic in the oxygen minimum zone in November 2014 and September 2013, respectively. Each float is equipped with two O_2 optodes, an unpumped Aanderaa 4330 optode (AADI, Bergen, Norway) and a pumped SBE63 optode (Sea-Bird Inc., Bellevue, USA). Aanderaa 4330 optodes have been pre-aged at the factory and were equipped with the standard foil with optical isolation. For each float, the optodes were laboratory-calibrated in the same calibration run (following Bittig et al., 2012) prior to deployment.

Only the unpumped Aanderaa 4330 optode, cable-mounted in an elevated position on the float's top cap, is capable of in-air measurements and the float's firmware was adjusted accordingly (see ~~Bittig and Körtzinger (2015)~~ Bittig and Körtzinger, 2015, for details). In addition, the Navis floats transmitted a timestamp for each profile sample ~~,~~ (i.e., each set of pressure, temperature, salinity, and optode raw data), through which only the time response analysis below was feasible. Since the Aanderaa optodes were mounted close to the floats' pumped-flow CTD intake, respectively, no additional compensation for a vertical pressure offset or a time delay was performed. A third float (WMO ID 6900891) was deployed in the South Pacific oxygen minimum zone off Peru in October 2015 but was trapped inactive near the surface for 5 weeks due to excess air in its air bladder before deployment. It eventually descended and started its mission, but the optodes failed after the first 30 profiles, so it was not included in the analysis.

3 Time Response

Bittig et al. (2014) used a set of laboratory experiments to validate a two-layer diffusional model of optode time response. In essence, water flow determines the liquid boundary layer thickness, l_L, in front of the optode's sensing foil, which is essentially independent of temperature. Temperature, however, modifies the O_2 solubility and diffusivity both in the boundary layer and sensing foil, such that the optode's response time, τ, shows a marked temperature dependence (at constant flow / l_L), being slower at low temperatures.

Shipboard CTD-O_2 casts with optodes, as well as glider and float data in different ocean regions served Bittig et al. (2014) to characterize the response time τ as well as the flow / l_L regime on these profiling platforms. However, while the shipboard casts had both a fast CTD-O_2 sensor and an O_2 optode on the same platform, the floats and gliders featured only a single optode and relied on a match of the optode data to a "nearby" CTD-O_2 profile. This match introduced some uncertainty into the analysis of Bittig et al. (2014). Using the dual-O_2 floats of the present study, the response time and boundary layer regime of optodes on slowly profiling platforms can be constrained far more tightly with the same methods.

Since the SBE63 optode's sensing foil is contained inside the pumped path of the float's CTD, its water flow is set by the pump speed of the float CTD, i.e., ca. 600 mL min^{-1} (Sea-Bird Electronics, 2016). This flow rate corresponds to a boundary layer thickness l_L around 34 μm (Bittig et al., 2014, see also Appendix A, eq. A4). The Aanderaa optode, however, is exposed to the ambient sea water and the flow in front of its sensing foil varies as a function of the platform's movement. Its flow (and thus its time response) is generally slower than for the pumped SBE63 optode.

Using the faster SBE63 optode O_2 as reference, the 4330 optode time response can be derived relative to the SBE63 optode. However, since the SBE63 optode's time response is well-defined (± 3 s) due to the pumped mode of operation, the results of Bittig et al. (2014) can be used to reconstruct a "true", time response-unbiased O_2 profile as reference. The 4330 optode time response can then be derived relative to that reference O_2 profile. Both approaches yield equivalent results and only the second one is shown below. Reconstruction of the unbiased O_2 profile is carried out as follows (see also Appendix/supplemental material):

– Define the flow regime for the pumped SBE63 optode, i.e., $l_L = 34$ μm.

– Translate the flow regime to a response time constant τ using the in-situ temperature and data from Fig. 11 in Bittig et al. (2014) (see also supplemental material).

– Obtain the mean of consecutive data points of the unbiased O_2 profile from the SBE63 optode measurements using the inverse of the filter's bilinear transformation, i.e., eq. 37 from Bittig et al. (2014) (eq. A3).

– Reconstruct the unbiased O_2 profile by interpolating the mean of consecutive data points of the unbiased O_2 profile to the original measurement times.

The analysis of the Aanderaa 4330 optode flow regime behaviour takes the opposite approach by filtering or "delaying" the reference O_2 profile until it matches the 4330 optode observations. For this, the forward filter (eq. 4 and 5 in Bittig et al., 2014,
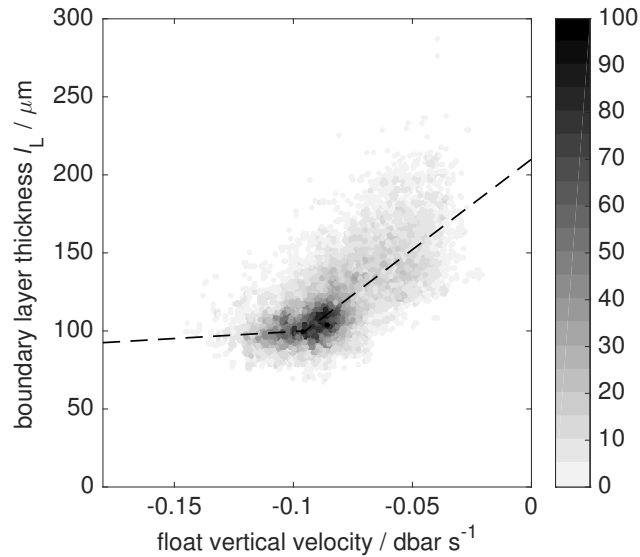
Figure 1. Boundary layer thickness l_L vs. float vertical velocity for an Aanderaa optode 4330 with standard foil derived from the dual-O_2 floats 6900889 and 6900890. The colour shading indicates the data density, while the dashed line gives the parameterization of equation 1

see also eq. A1 and A2) was applied to a short interval of the unbiased O_2 profile and l_L iteratively adjusted. The steps involved are essentially:

– Estimate a boundary layer thickness l_L for the given short interval of measurements (here: 12 consecutive data points).

– Translate l_L to a response time constant τ using the in-situ temperature and data from Fig. 11 in Bittig et al. (2014) (see also supplemental material).

– Translate τ to the filter constants a and b using the measurement times t_i and eq. 4 from Bittig et al. (2014) (eq. A1).

– Apply the recursive filter to the mean of consecutive data points of the unbiased O_2 profile and the previous (or inital) filtered O_2 measurement (eq. 4 and 5 in Bittig et al., 2014) (eq. A1 and A2).

– Compare the filtered O_2 profile with the Aanderaa 4330 optode measurements and iteratively refine the chosen boundary layer thickness l_L for the given short interval until a best match is achieved.

Overall, the resulting boundary layer thickness l_L is smaller than estimated by Bittig et al. (2014). l_L decreases with increased flow at the sensor as expected (figure 1). Specifically, l_L is around 210 µm at 0 $\mathrm{dbar\,s^{-1}}$ and 100 µm at 0.095 $\mathrm{dbar\,s^{-1}}$. However, there appears to be a lower limit or regime shift at speeds higher than 0.1 $\mathrm{dbar\,s^{-1}}$, likely reflecting the transition between laminar and turbulent flow at the sensing foil. From CTD applications, Bittig et al. (2014) found a l_L around 20 µm at 1.0 $\mathrm{dbar\,s^{-1}}$ when the flow was directed approx. perpendicular to the optode sensing foil (as is typically the case for floats). For other CTD applications with the flow passing tangentially along the optode ~~sensing foil~~ (similar to typical glider optode
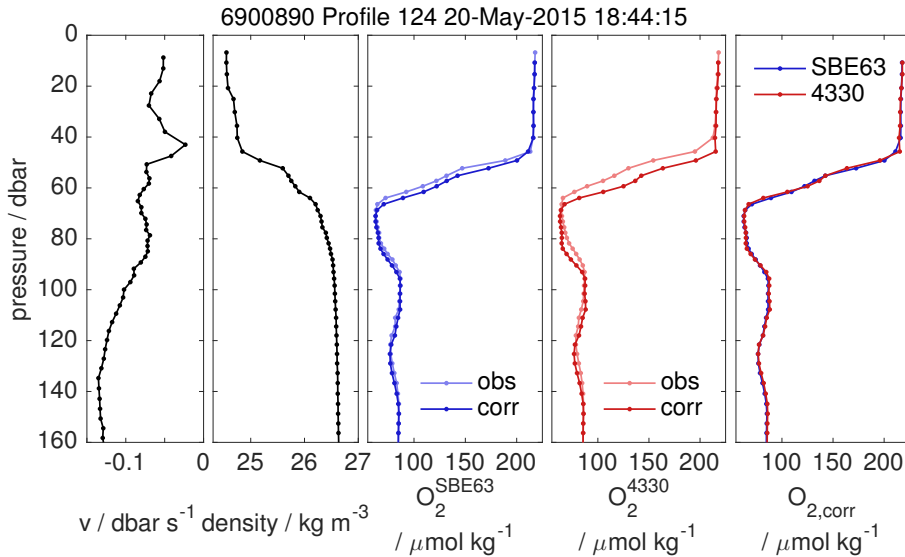
Figure 2. ~~Profile~~ Profiles of ascent speed, density, SBE63 optode O₂, 4330 optode O₂, and time response-corrected O₂ (left to right; outer right panel shows the superposition of corrected O₂ for the SBE63 and 4330 optode from the previous panels) for float 6900890, cycle 0124. The main oxycline coincides with the pycnocline and the float slows down significantly around 50 dbar, giving the O₂ optodes time to adjust. After correction, both sensors agree well in the profile fine structure and the depth of the oxycline, while they diverge before. The time response effect is more pronounced in regions with a weaker density gradient.

attachments), l_L was close to 40 μm at 1.0 dbar s^{-1} (Bittig et al., 2014). Using these endmembers, we chose a piecewise linear interpolation to parameterize the flow regime / l_L vs. platform speed v for floats (equation 1). For gliders, we suggest equation 2, accordingly.

$$l_L(\text{float})/\upmu\text{m} = \begin{cases} 210 - \frac{110}{0.095} \cdot \left|v/\text{dbar s}^{-1}\right| & |v| \le 0.095 \text{ dbar s}^{-1} \\ 20 + \frac{80}{0.905} \cdot \left(1 - \left|v/\text{dbar s}^{-1}\right|\right) & |v| > 0.095 \text{ dbar s}^{-1} \end{cases} \tag{1}$$

$$l_L(\text{glider})/\upmu\text{m} = \begin{cases} 210 - \frac{110}{0.095} \cdot \left|v/\text{dbar s}^{-1}\right| & |v| \le 0.095 \text{ dbar s}^{-1} \\ 40 + \frac{60}{0.905} \cdot \left(1 - \left|v/\text{dbar s}^{-1}\right|\right) & |v| > 0.095 \text{ dbar s}^{-1} \end{cases} \tag{2}$$

This flow regime characterization can now be used to reconstruct a time response-unbiased O₂ profile from the Aanderaa 4330 optode the same way as for the SBE63 optode. It is to stress, however, that all time response corrections need to be done on a time axis ("timeseries"), not on a pressure axis ("depth profile"). It is therefore important that a time stamp is logged with each optode measurement.

An example of such a reconstruction is shown in figure 2, while figure 3 illustrates the time response effect. Both floats were deployed in a tropical region with a strong thermo- and consequently pycnocline (panel 3a ~~). Accordingly,~~ and figure 2). The density structure determines the floats' ascent velocity and the float slows down significantly in the ~~subsurface~~ main
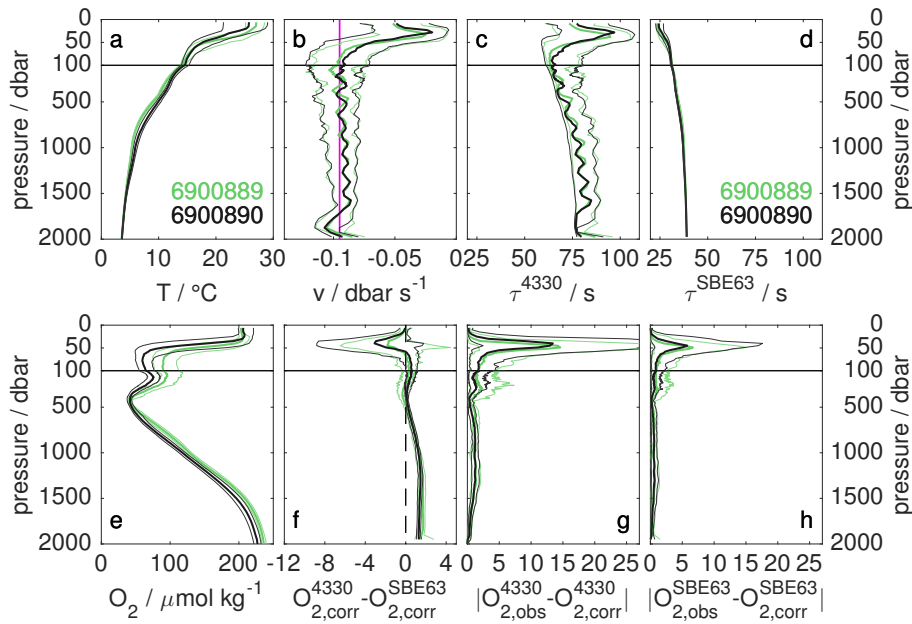
Figure 3. Median profiles (thick line) with 10/90-percentiles (thin lines) for float 6900889 (green) and 6900890 (black): (a) temperature, (b) ascent ~~speed~~velocity with l_L vs. v regime transition (eq. 1) in purple, (c) response time τ of the Aanderaa 4330 optode, (d) response time τ of the SBE63 optode, (e) oxygen profile, (f) difference between time response-corrected 4330 optode and SBE63 optode O_2 as a measure of sensor agreement after correction (in μmol kg^{-1}), (g) absolute difference between observed and time response-corrected O_2 as a measure of the time response bias for the Aanderaa 4330 optode (in μmol kg^{-1}), (h) absolute difference between observed and time response-corrected O_2 as a measure of the time response bias for the SBE63 optode (in μmol kg^{-1}).

thermo- and pycnocline around 50 dbar (3b). At intermediate and deep depths, a stable density structure seems to cause the float's buoyancy adjustments (i.e., change in oil bladder volume to keep a certain ascent velocity) to occur at similar depths for all profiles, which creates the wavelike fluctuations in the median float velocity. Moreover, the l_L - v dependence regime transition at 0.095 dbar s^{-1} is close to the median float velocity. Observations faster than this threshold have an l_L of essentially
5 $100-110$ µm, while observations at slower velocities show a marked v dependence (compare fig. 1). This is mirrored in the boundary layer thickness of the unpumped 4330 optode (not shown) ~~, causing~~and in its response time (3c). The slowdown in the main pycnocline causes a 50 % increase in response time of the 4330 optode (from 60 s to 95 s), while the pumped SBE63 optode remains unaffected (ca. $25-30$ s). Superimposed to the flow effect, cold temperatures at depth cause an increase in τ (3c and 3d). It is important to note that τ is much better constrained for the pumped SBE63 optode than for the unpumped
10 4330 optode.

As expected, time response correction for the pumped SBE63 optode with small response times changes the O_2 data only to some extent (median absolute difference in the strongest gradient: ~~6—8~~$6-7$ µmol kg^{-1}; 3h) and is much more important for the unpumped 4330 optode with larger response times (~~13—17~~$13-15$ µmol kg^{-1}; 3g). After correction, both sensors

agree to within $2-3\,\mathrm{\mu mol\,kg^{-1}}$ (median difference) in the strongest gradient region ($120\,\mathrm{\mu mol\,kg^{-1}}$ change over 8 minutes or $20\,\mathrm{dbar}$) and better elsewhere (3f). Especially near the surface and in the core of the oxygen minimum zone, the difference is close to zero. However, there is a residual pressure effect between the sensors of ca. $2\,\mathrm{\mu mol\,kg^{-1}}$ at $2000\,\mathrm{dbar}$ (3f), in line with a pressure correction uncertainty of $0.3\,\%$ per $1000\,\mathrm{dbar}$ each (Bittig et al., 2015a).

This demonstrates that a time response correction is both useful to remove sensor artifacts (3g, 3h) and feasible for both optode models, yielding highly consistent results (3f). It is, however, only possible if the respective measurement times are known, i.e., provided by the manufacturer through the instrument's firmware as well as transmitted or stored in the data stream.

Interestingly, a similar analysis on the limited dataset of the third float, WMO ID 6900891, yields apparent boundary layer thicknesses l_L for the 4330 optode that are $100\,\mathrm{\mu m}$ or more higher. We believe this is caused by growth of a biofilm on the sensing foil during its 5-week irregular near-surface drift, which artificially delays the time response. The SBE63 optode, being contained in the CTD's pumped path and antifouling regime, is probably better protected against such artifacts.

4   In-Air Measurements

The feasibility to calibrate O_2 optodes on floats by measurements in-air, proposed by Körtzinger et al. (2005), was first demonstrated by Fiedler et al. (2013). Bittig and Körtzinger (2015) showed the first long time series of in-air measurements over 15 months using a single float. ~~They~~ There, we demonstrated a systematic effect of any water-side oxygen disequilibrium on near-surface in-air measurements, that can and needs to be corrected. Subsequently, Johnson et al. (2015) confirmed the consistency between in-air and in-situ calibrations for a fleet of floats, while Bushinsky et al. (2016) showed the utility of several in-air data acquisitions per surfacing, a daytime dependence, and the potential for in-situ drift detection.

Bittig and Körtzinger (2015) used the then available ca. 15 months of data for float 6900890. Here, we want to expand ~~their~~ our analysis to all data until ~~August~~ December 2016 and apply it to both dual-O_2 floats 6900889 and 6900890 (i.e., ~~21 and 34~~ 25 and 38 months, respectively). Both floats show a similar "carry-over" slope c of ~~0.21 and~~ 0.23, ~~respectively,~~ similar to Bittig and Körtzinger (2015) and Johnson et al. (2015). Using this value, we can compensate for the surface water contamination of the in-air measurements and derive an oxygen correction factor m_i (or gain factor g_i as in Johnson et al., 2015) for each profile i (figure 4), where $pO_{2,\mathrm{obs}}$ is the uncalibrated optode O_2 partial pressure (or O_2 saturation or O_2 concentration) and $pO_{2,\mathrm{corr}}$ is the calibrated O_2:

$$m = \frac{pO_{2,\mathrm{corr}}}{pO_{2,\mathrm{obs}}} \tag{3}$$

In contrast to Bittig and Körtzinger (2015), the longer float time series confirm the results from Bushinsky et al. (2016), i.e., the existence of a small but significant in-situ drift of the optode (loss in O_2 sensitivity of ~~0.2 − 0.4~~ 0.27 − 0.40 % per year) as well as a daytime dependence of the in-air measurements. Over the course of the day, correction factors decrease, i.e., optode in-air measurements apparently increase, by roughly $1\,\%$ between $7\,\mathrm{h}$ and $17\,\mathrm{h}$ local time, which is in the same direction but of slightly smaller magnitude than their findings (figure 5).
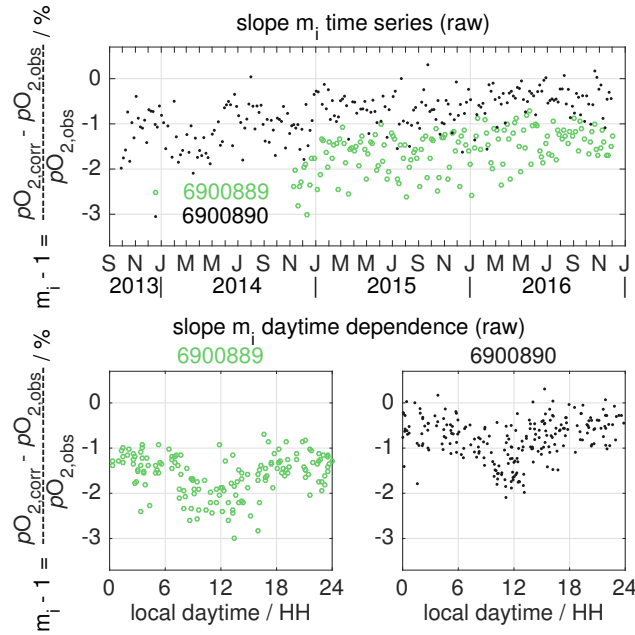
Figure 4. Time series (top) as well as daytime dependence (bottom) of the oxygen correction slope m_i from in-air measurements for float 6900889 (grey circles) and 6900890 (black dots). m_i was calculated for each in-air measurement by compensating the surface water contamination with a uniform "carry-over" slope c for the entire deployment. There is a trend towards higher correction factors m_i with time, indicating a small drift of the optodes to lower sensitivity. Daytime has a noticeable effect on in-air measurements with correction factors m_i being decreased during the day by about 1 %, i.e., the optode readings being apparently increased. Both effects, the in-situ drift and daytime dependence, act in parallel and are superimposed in the data presented here.

One can postulate that the daytime bias is related to solar heating of the sensor's sensing foil and thus the solar elevation angle θ. In that case, the daytime effect Δm_i would correlate on average with the cosine of the zenith angle (eq. 4).

$$\Delta m_i(\theta_i) \; \propto \; \cos\left(90° - \theta_i\right) = \sin\theta_i \tag{4}$$

If the bias is caused by the energy input to the float top cap, the daytime effect would be related to the direct sun irradiance, which is a function of the sun light's attenuation in the atmosphere (Meinel and Meinel, 1976, eq. 5),

$$\Delta m_i(\theta_i) \; \propto \; 0.7^{\mathrm{AM}^{0.678}} \quad , \text{with AM} = \sqrt{\left(\frac{6371}{9} \cdot \sin\theta_i\right)^2 + 2 \cdot \frac{6371}{9} + 1} - \frac{6371}{9} \cdot \sin\theta_i \tag{5}$$

where AM is the air mass coefficient for the path length through the atmosphere, modelled as a spherical shell of 9 km around the Earth (radius 6371 km). The data can be adequately described by both approaches. We thus used the solar elevation angle θ and the simpler equation 4 to parameterize the daytime dependence (eq. 6),

$$m_i(\theta_i) = \begin{cases} m_0 & \theta_i \leq \theta_c \\ m_0 + m_A \cdot \frac{\sin\theta_i - \sin\theta_c}{1 - \sin\theta_c} & \theta > \theta_c \end{cases} \tag{6}$$
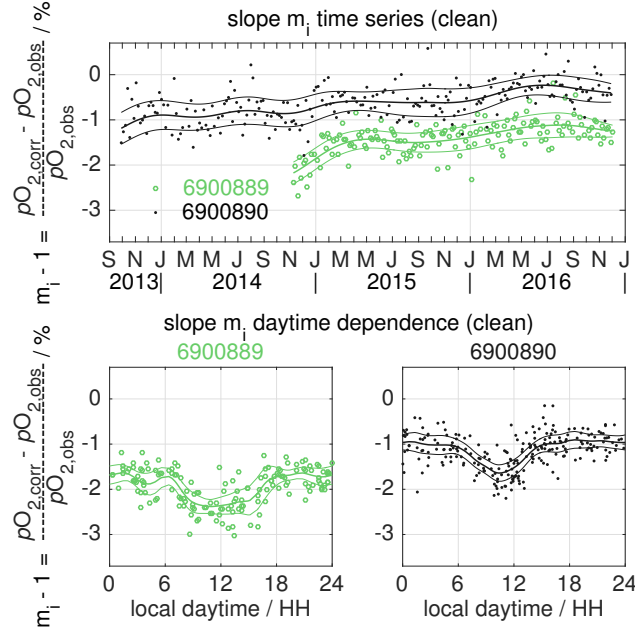
Figure 5. Same as figure 4 except that the daytime dependence was removed from the time series (eq. 6, $\theta_c = 15°$; top panel) and the in-situ drift removed from the daytime dependence (eq. 7; bottom panel). Thick lines give a 6 months (time series) and 3 hours (daytime dependence) low-pass filtered trend with $\pm 2\sigma$ as thin lines. The m_i low-bias during mid-day is an important contributor to the average in-air correction (compare the time series of m_i without and with compensation of the daytime dependence, figure 4 and 5, top panel, respectively) and needs to be considered.

where θ_c is the critical solar elevation angle below which correction factors m_i are uniform and equal to m_0 and m_A is the amplitude of the mid-day bias. Based on the available data, we set θ_c to $15°$. The in-situ optode sensitivity drift is parameterized as a linear drift according to:

$$m_i(\Delta t_i) = m_{t=0} + a \cdot \frac{\Delta t_i}{365 \text{ d}} \tag{7}$$

5 where Δt_i is the time since deployment (in days) for each profile i and a is the annual drift rate in $\% \text{ yr}^{-1}$. If enough data are available (as in our case), the linear carry-over (see Bittig and Körtzinger, 2015, eq. 10), the daytime dependence (eq. 6), and the in-situ drift (eq. 7) can be fit simultaneously (with fit parameters c, $m_{t=0}$, m_A, and a) to correct all effects at once and obtain an optimal fit (eq. 8).

$$pO_{2,\text{obs},i}^{\text{infl}} = c \cdot pO_{2,\text{obs},i}^{\text{defl}} + \frac{1-c}{m_i(\theta_i, \Delta t_i)} \cdot pO_{2,\text{air},i} \tag{8}$$

10 Consequently, data can be corrected by:

$$pO_{2,\text{corr},i} = m_i(\theta_i, \Delta t_i) \cdot pO_{2,\text{obs},i} = \begin{cases} \left(m_{t=0} + a \cdot \frac{\Delta t_i}{365 \text{ d}}\right) \cdot pO_{2,\text{obs},i} & \theta_i \leq \theta_c \\ \left(m_{t=0} + a \cdot \frac{\Delta t_i}{365 \text{ d}} + m_A \cdot \frac{\sin\theta_i - \sin\theta_c}{1 - \sin\theta_c}\right) \cdot pO_{2,\text{obs},i} & \theta > \theta_c \end{cases} \tag{9}$$

Table 1. Simultaneous fit of "carry-over" slope c, initial O_2 correction factor $m_{t=0}$ relative to the deployment calibration, daytime dependence amplitude m_A, and annual drift rate a (eq. 8) for floats 6900889 and 6900890 using air pO_2 derived from different reanalysis models. The analysis was limited to all profiles until the most recently available ERA-Interim date, i.e., ~~July~~ Sept. 2016.

Float	Reanalysis	c	$m_{t=0} = \left.\frac{pO_{2,\text{corr}}}{pO_{2,\text{deploy}}}\right\|_{t=0}$	m_A in %	a in % yr^{-1}
6900889	NCEP/NCAR	~~0.20(0.05)~~ 0.21(0.05)	~~0.9825(0.0013)~~ 0.9821(0.0012)	~~−0.92(0.17)~~ −0.79(0.15)	~~+0.40(0.14)~~ +0.42(0.11)
	ERA-Interim	~~0.21(0.05)~~ 0.22(0.04)	~~0.9839(0.0012)~~ 0.9836(0.0011)	~~−0.93(0.16)~~ −0.79(0.15)	~~+0.39(0.14)~~ +0.40(0.11)
	MERRA2	~~0.21(0.05)~~ 0.23(0.05)	~~0.9843(0.0014)~~ 0.9839(0.0013)	~~−1.02(0.18)~~ −0.81(0.17)	~~+0.36(0.15)~~ +0.36(0.12)
	JRA-55	~~0.24(0.05)~~ 0.24(0.04)	~~0.9841(0.0013)~~ 0.9838(0.0012)	~~−1.11(0.17)~~ −0.93(0.16)	~~+0.41(0.15)~~ +0.40(0.11)
6900890	NCEP/NCAR	0.23(0.02)	~~0.9907(0.0013)~~ 0.9899(0.0012)	~~−0.62(0.14)~~ −0.53(0.13)	~~+0.19(0.07)~~ +0.24(0.06)
	ERA-Interim	0.23(0.02)	~~0.9901(0.0013)~~ 0.9894(0.0012)	~~−0.66(0.14)~~ −0.58(0.13)	~~+0.26(0.07)~~ +0.29(0.05)
	MERRA2	0.21(0.02)	~~0.9911(0.0014)~~ 0.9905(0.0012)	~~−0.57(0.15)~~ −0.49(0.13)	~~+0.22(0.08)~~ +0.25(0.06)
	JRA-55	0.24(0.02)	~~0.9897(0.0014)~~ 0.9894(0.0012)	~~−0.59(0.15)~~ −0.54(0.13)	~~+0.28(0.08)~~ +0.29(0.06)

95 % confidence interval given in brackets; $\theta_c = 15°$

For simple calibration, however, preference should be given to dusk, nighttime, and dawn measurements ($\theta_i \leq \theta_c$), where the (yet uncharacterized) amplitude m_A of the daytime dependence is irrelevant (eq. 6).

For float 6900889, m_A is ca. ~~1~~0.8 %, while it is around ~~0.6~~0.5 % for float 6900890 (table 1). Both floats show a significant in-situ drift: O_2 levels decrease by ~~−0.4~~−0.40 % yr^{-1} and ~~−0.2~~−0.27 % yr^{-1}, respectively, with the 95 % confidence level being around ~~0.15~~0.11 % yr^{-1} after 2 years of float data ~~, and below 0.1~~and around 0.06 % yr^{-1} after three years. The "carry-over" slope c of float 6900889, operating in open ocean waters, is not as tightly constrained as for 6900890, operating closer to coastal and upwelled waters, where the range of oxygen super- and undersaturation is larger. When accounting for the surface water "carry-over" effect only, fit root mean squared errors (RMSE) are around 0.8 mbar (Bittig and Körtzinger, 2015). With all effects included, the RMSE is reduced to 0.5 mbar. The intercept $m_{t=0}$ gives an indication of the uncertainty in m_i after daytime and drift correction, which is on the order of 0.1 %.

To evaluate the sensitivity to the atmospheric reanalysis product, air pO_2 was derived from NCEP/NCAR (Kalnay et al., 1996), ERA-Interim (Dee et al., 2011), MERRA-2 (Rienecker et al., 2011), and JRA-55 (Harada et al., 2016) reanalysis data. ERA-Interim has a delay of 2-3 months, so the analysis was limited to all profiles until July 2016 (table 1). Differences in $m_{t=0}$ are up to $0.1 - 0.2$ % depending on the reanalysis model and as such on the same order of magnitude as the uncertainty of the calculation. This should be considered when assessing the absolute calibration accuracy of in-air data. Differences for c, m_A, and a are within their confidence intervals.
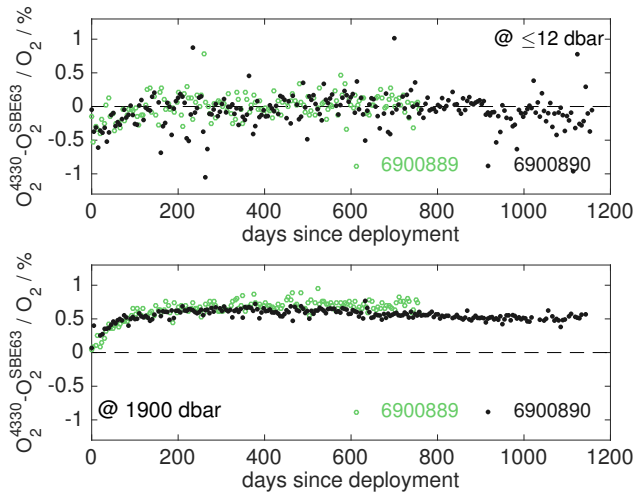
Figure 6. Percent difference between O_2 from the Aanderaa 4330 optode and the SBE63 optode using time response corrected data (top) near the surface and (bottom) at depth for float 6900889 (grey) and 6900890 (black). There seems to be a conditioning effect on either one (or both) optodes during the first half year / ≈ 40 profiles, after which differences between optodes are stable.

5 Optode Stability

Based on regular in-air measurements, the Aanderaa 4330 optodes show a significant drift of ~~−0.4~~ −0.40 % yr^{-1} and ~~−0.2~~ −0.27 % yr^{-1} for float 6900889 and 6900890, respectively. This is in a similar range for in-situ drift as reported by Bushinsky et al. (2016) for 10–12 out of 14 optodes. In contrast, Johnson et al. (2015) ~~did not find a significant drift when looking at~~ observed

5 both significant positive and negative drifts for individual floats but seen over a fleet of 29 floats, that drift was indistinguishable from zero. However, ~~instead of trying to compensate for the surface water contamination as Bittig and Körtzinger (2015), they used only that subset of data where the contamination is expected~~ they did not correct explicitly for the carry over effect but, given that O_2 is typically less than 3 % ~~supersaturated, assumed it~~ to be negligible ~~. One can speculate that if all data were used, they might have found a statistically significant drift~~ as long as the data record spans at least a full year.

10   Since the SBE63 optode on floats can not measure oxygen in-air, a direct comparison with in-air measurements is not possible. However, it can be done indirectly via the difference between the 4330 and the SBE63 optode (figure 6), both near the surface within the mixed layer as well as at depth (1900 dbar). The SBE63s have been in-situ calibrated against the 4330 optodes near the surface, so differences cluster around zero with a standard deviation of 0.2 %. At depth, however, there is a difference between both on the order of 0.5 %, which we attribute to uncertainties in the pressure correction (Bittig et al.,

15 2015a).

Moreover, at both depths, there seems to be a conditioning effect during the first half year (≈ 40 profiles) only after which the difference between both sensors stabilizes. Since we can only discuss the difference, this can be caused by either one or both sensors. Reasons could be repeated pressure cycling, removal of surface films or contaminants from the sensing foils,

or others, and the exact cause remains speculative. However, we recommend that users critically evaluate their optode data whether they see such a conditioning artifact, too.

Linear fit slopes of the sensor difference (using only data after 180 days) for the two floats are indistinguishable from zero within ~~±0.1 and ±0.05~~ ±0.06 and ±0.04 % yr^{-1} (95 % CI), respectively. This implies ~~,~~ that the SBE63 optodes drift as

5   much as the 4330 optodes and suggests that in-situ drift is governed by environmental factors. _Concerning the different in situ drift rate between the two floats, the only obvious difference is that the second pair of optodes was deployed a year later and subjected to a second laboratory calibration before deployment. Otherwise, they were from the same batch, treated the same, and the floats were deployed in comparable field conditions._

6   Conclusions

10   A slow O_2 time response reduces fine scale resolution and causes a lag between in-situ and observed O_2 profile. It is important for data users to assess and to quantify the impact on O_2 data quality, as the effect can be substantial for the analysis (e.g., Plant et al., 2016). However, as demonstrated by Bittig et al. (2014) and here, it is feasible to correct for the time response effect on slowly-moving, buoyancy-driven platforms. In this work, we ~~refined~~ refine the flow regime required for such corrections for floats and gliders and ~~summarized~~ summarize the procedure for time response corrections (from Bittig et al.,

15   2014). Reconstruction, however, is only possible if measurement times are known. ~~They~~ These need to be provided by the instrument's firmware/manufacturer as well as being transmitted and stored with the original profile data. Of course, every correction introduces uncertainty, so the ideal case would be a fast (and accurate) O_2 sensor that doesn't need time response correction.

In-air measurements at every surfacing of Argo-O_2 floats prove to be an ideally-suited mean to check and correct a change

20   (or loss) in O_2 sensitivity of optodes, the primary reason of O_2 optode drift (Bittig and Körtzinger, 2015). As such, they allow both to correct sensor drift between calibration and deployment (several % magnitude) as well as sensor drift in-situ during deployment (order of -0.5 % yr^{-1}). In detail, measurements in air close to the sea surface are not purely 100 % air as one would expect under controlled, stable conditions. Most ~~prominently~~importantly, any water-side oxygen disequilibrium has a systematic effect on near-surface in-air measurements, that can and needs to be corrected. In addition, mid-day observations

25   are offset with respect to night time or dusk and dawn measurements, such that a failure to account for the daytime effect introduces a systematic bias. While its mechanistic origin is still unclear, the data suggests a relation to solar heating. Despite these secondary effects, any float O_2 data calibrated with regular in-air measurements is more accurate than without in-air measurements (compare Takeshita et al., 2013), but neglecting the water-side "carry-over" or daytime effect should be avoided as good practice.

30   Based on regular in-air measurements over ~~34 and 21~~ 38 and 25 months, respectively, we were able to detect a significant in-situ drift in both 4330 optodes of ~~-0.2 and -0.4~~-0.27 and -0.40 % yr^{-1}, respectively. The SBE63 optodes' in-situ stability is comparable to the one of the 4330 optodes.

Given the findings of several studies on both optode "storage" drift and in-situ drift, we strongly propose that every Biogeochemical-Argo float be deployed with in-situ O_2 optode in-air measurements ~~(SCOR WG 142, 2016)~~(Bittig et al., 2015b). Float-PIs need to ensure with manufacturers that their floats provide this capability.

To our knowledge, the feasibility of in-air measurements on gliders still needs to be shown. Given the ~~in general~~ generally shorter deployment periods and, more importantly, the possibility for careful pre- and post-deployment calibration / drift characterization (e.g., by optode in-air measurements under controlled conditions on deck), it might not be necessary to have in-situ in-air measurements on gliders.

Appendix A: Time Response Correction

Here, we reproduce the essential equations from Bittig et al. (2014) for the correction of the optode time response as demonstrated in section 3, give an explicit parameterization for the flow – boundary layer thickness relation for optodes in pumped mode of operation, and provide the two-layer diffusional model data to relate boundary layer thickness, temperature, and response time for interpolation as supplemental material. We hope this to be ~~easier accessible and~~ more useful than the solely graphical representation of Bittig et al. (2014).

The O_2 optode's time response is governed by the diffusion of O_2 in/out of the sensing foil and trough the liquid boundary layer in front of the sensing foil. In fact, the boundary layer is responsible for most of the "lag". The step response follows (approx.) an exponential curve. The continuous time response equals a single-pole low-pass filter of the in-situ O_2 time series. In discrete form using the bilinear transformation, this filter is recursively described by

$$c^{\text{obs}}(t_{i+1}) = a \cdot c^{\text{obs}}(t_i) + b \cdot \left(c^{\text{in-situ}}(t_{i+1}) + c^{\text{in-situ}}(t_i)\right), \qquad a = 1 - 2b, \quad b = \left(1 + 2\frac{\tau}{t_{i+1} - t_i}\right)^{-1} \tag{A1}$$

$$c^{\text{obs}}(t_{i=0}) = c^{\text{in-situ}}(t_{i=0}) \tag{A2}$$

where $c^{\text{in-situ}}$ is the true in-situ O_2 time series, c^{obs} the O_2 time series of the optode, and τ the response time for the interval between t_i and t_{i+1}. The initial condition (eq. A2) assumes an equilibrated optode, which can be adjusted according to the application.

For the reconstruction, eq. A1 is rearranged to

$$\frac{c^{\text{in-situ}}(t_{i+1}) + c^{\text{in-situ}}(t_i)}{2} = \frac{1}{2b} \cdot \left(c^{\text{obs}}(t_{i+1}) - a \cdot c^{\text{obs}}(t_i)\right), \qquad a = 1 - 2b, \quad b = \left(1 + 2\frac{\tau}{t_{i+1} - t_i}\right)^{-1} \tag{A3}$$

i.e., knowledge of the optode time series (measurement times, t_i, and optode readings, c^{obs}) as well as the response time (series) τ yields a time series of the consecutive means of the true in-situ time series (left side of eq. A3). For this operation, no initial condition of the filter is required. To obtain the in-situ time series at the original sampling times t_i, the time series of consecutive means obtained from eq. A3 needs to be interpolated to t_i.

For a pumped optode, the relation between flow $\dot{V}$ and boundary layer thickness l_L is described (after experiment **1**, Bittig et al., 2014) by

$$l_L(\text{pumped})\,/\,\mu\text{m} = 1.8 \cdot 10^4 \cdot \frac{1}{\dot{V}\,/\,\text{mL min}^{-1}} + 4 \tag{A4}$$

with an uncertainty of the greater of 4 μm or 10 %.

5   For unpumped optodes on fast profiling platforms, i.e., CTDs, the vertical velocity v – boundary layer thickness l_L relation depends to a large extent on the mode and orientation of attachment (see difference between experiment **5** and **6**, Bittig et al., 2014) with a range of $l_L(\text{CTD})$ from 20 μm to 55 μm (1σ from 5 μm to 35 μm). For slowly profiling platforms, we suggest to use eq. 1 for floats and eq. 2 for gliders. They might need adjustments depending on the actual optode attachment or mode of operation.

10   The boundary layer thickness l_L can be converted to a response time τ using the sensing membrane thickness l_M of the respective optode model, the two-layer diffusional model of Bittig et al. (2014), and temperature T. For the SBE63 optode, they used $l_M = 130$ μm, for the Aanderaa 3830/4330 optode with standard foil 100 μm, and for the Aanderaa 4330F optode with fast response foil 50 μm. Results for the latter two were shown in ~~their~~ figure 11, Bittig et al. (2014). Here, the same model data of τ against l_L and T can be found for all three optode sensing foils in the supplemental material.

15   *Acknowledgements.* The authors want to thank Patrice Brehmer (IRD, Dakar, Senegal) as well as the captain and crew of M/V *Samba Laobé Fall* cruise AWARGO for help with the deployment of 6900890, Tobias Hahn (GEOMAR, Kiel, Germany) as well as the captain, crew, and scientists of R/V *Polarstern* cruise PS88.2 for the deployment of 6900889, and Sea-Bird Electronics for their efforts with float and firmware customization. The float data are made freely available by the International Argo Program (Argo, 2000) and the national programs that contribute to it (http://www.argo.ucsd.edu, http://argo.jcommops.org). The Argo Program is part of the Global Ocean

20 Observing System. NCEP Reanalysis data provided by the NOAA/OAR//OAR/ESRL PSD, Boulder, Colorado, USA, from their Web site at http://www.esrl.noaa.gov/psd//psd/, ERA-Interim data provided courtesy ECMWF, MERRA2 data files acquired from the Goddard Earth Science Data Information Services Center (GES DISC), and JRA-55 data provided from the Japanese 55-year Reanalysis (JRA-55) project carried out by the Japan Meteorological Agency (JMA). Financial support by the following projects is gratefully acknowledged: AtlantOS (EU Horizon 2020 Grant Agreement 2014-633211), remOcean (EU ERC Grant Agreement 246777), and E-AIMS (EU FP7 Project 312642),

25 as well as O_2-Floats (KO 1717/3-1) and the SFB754 of the German Science Foundation (DFG).

References

Argo: Argo float data and metadata from Global Data Assembly Centre (Argo GDAC), doi:10.17882/42182, 2000.

Bittig, H. C. and Körtzinger, A.: Tackling oxygen optode drift: Near-surface and in-air oxygen optode measurements on a float provide an accurate in situ reference, J. Atmos. Oceanic Technol., 32, 1536–1543, doi:10.1175/JTECH-D-14-00162.1, 2015.

5 Bittig, H. C., Fiedler, B., Steinhoff, T., and Körtzinger, A.: A novel electrochemical calibration setup for oxygen sensors and its use for the stability assessment of Aanderaa optodes, Limnol. Oceanogr.: Methods, 10, 921–933, doi:10.4319/lom.2012.10.921, 2012.

Bittig, H. C., Fiedler, B., Scholz, R., Krahmann, G., and Körtzinger, A.: Time response of oxygen optodes on profiling platforms and its dependence on flow speed and temperature, Limnol. Oceanogr.: Methods, 12, 617–636, doi:10.4319/lom.2014.12.617, 2014.

Bittig, H. C., Fiedler, B., Fietzek, P., and Körtzinger, A.: Pressure Response of Aanderaa and Sea-Bird Oxygen Optodes, J. Atmos. Oceanic
10 Technol., 32, 2305–2317, doi:10.1175/JTECH-D-15-0108.1, ~~2015.~~ 2015a.

~~SCOR WG 142~~Bittig, H. C., Körtzinger, A., Johnson, K. S., Claustre, H., Emerson, S., Fennel, K., Garcia, H., Gilbert, D., Gruber, N., Kang, D.-J., Naqvi, W., Prakash, S., Riser, S., Thierry, V., Tilbrook, B., Uchida, H., Ulloa, O., and Xing, X.: SCOR WG 142: Recommendation for Oxygen Measurements from Argo Floats: Implementation of In-Air-Measurement Routine to Assure Highest Long-term Accuracy, doi:10.13155/45917, ~~2016~~2015b.

15 Bushinsky, S. M., Emerson, S. R., Riser, S. C., and Swift, D. D.: Accurate oxygen measurements on modified Argo floats using in situ air calibrations, Limnol. Oceanogr.: Methods, doi:10.1002/lom3.10107, 2016.

D'Asaro, E. A. and McNeil, C.: Calibration and Stability of Oxygen Sensors on Autonomous Floats, J. Atmos. Oceanic Technol., 30, 1896–1906, doi:10.1175/JTECH-D-12-00222.1, 2013.

Dee, D. P., Uppala, S. M., Simmons, A. J., Berrisford, P., Poli, P., Kobayashi, S., Andrae, U., Balmaseda, M. A., Balsamo, G., Bauer, P.,
20 Bechtold, P., Beljaars, A. C. M., van de Berg, L., Bidlot, J., Bormann, N., Delsol, C., Dragani, R., Fuentes, M., Geer, A. J., Haimberger, L., Healy, S. B., Hersbach, H., Hólm, E. V., Isaksen, L., Kållberg, P., Köhler, M., Matricardi, M., McNally, A. P., Monge-Sanz, B. M., Morcrette, J.-J., Park, B.-K., Peubey, C., de Rosnay, P., Tavolato, C., Thépaut, J.-N., and Vitart, F.: The ERA-Interim reanalysis: configuration and performance of the data assimilation system, Q. J. R. Meteorol. Soc., 137, 553–597, doi:10.1002/qj.828, 2011.

Fiedler, B., Fietzek, P., Vieira, N., Silva, P., Bittig, H. C., and Körtzinger, A.: In Situ CO2 and O2 Measurements on a Profiling Float, J.
25 Atmos. Oceanic Technol., 30, 112–126, doi:10.1175/JTECH-D-12-00043.1, 2013.

Harada, Y., Kamahori, H., Kobayashi, C., Endo, H., Kobayashi, S., Ota, Y., Onoda, H., Onogi, K., Miyaoka, K., and Takahashi, K.: The JRA-55 Reanalysis: Representation of Atmospheric Circulation and Climate Variability, J. Meteor. Soc. Japan, 94, 269–302, doi:10.2151/jmsj.2016-015, 2016.

Johnson, K. S. and Claustre, H.: ~~Planning for a~~ Bringing ~~Global~~Biogeochemistry into the ~~Biogeochemical~~ Argo ~~Program~~Age, Eos~~Trans.~~
30 ~~AGU, in press~~, 97, doi:10.1029/2016EO062427, 2016.

Johnson, K. S., Plant, J. N., Riser, S. C., and Gilbert, D.: Air Oxygen Calibration of Oxygen Optodes on a Profiling Float Array, J. Atmos. Oceanic Technol., 32, 2160–2172, doi:10.1175/JTECH-D-15-0101.1, 2015.

Kalnay, E., Kanamitsu, M., Kistler, R., Collins, W., Deaven, D., Gandin, L., Iredell, M., Saha, S., White, G., Woollen, J., Zhu, Y., Leetmaa, A., Reynolds, R., Chelliah, M., Ebisuzaki, W., Higgins, W., Janowiak, J., Mo, K. C., Ropelewski, C., Wang, J., Jenne,
35 R., and Joseph, D.: The NCEP/NCAR 40-Year Reanalysis Project, Bull. Amer. Meteor. Soc., 77, 437–471, doi:10.1175/1520-0477(1996)077<0437:TNYRP>2.0.CO;2, 1996.

Körtzinger, A., Schimanski, J., and Send, U.: High Quality Oxygen Measurements from Profiling Floats: A Promising New Technique, J. Atmos. Oceanic Technol., 22, 302–308, doi:10.1175/JTECH1701.1, 2005.

Meinel, A. B. and Meinel, M. P.: Applied Solar Energy: An Introduction, Addison-Wesley Pub. Co., 1976.

Plant, J. N., Johnson, K. S., Sakamoto, C. M., Jannasch, H. W., Coletti, L. J., Riser, S. C., and Swift, D. D.: Net community production at Ocean Station Papa observed with nitrate and oxygen sensors on profiling floats, Global Biogeochem. Cycles, 30, 859–879, doi:10.1002/2015GB005349, 2016.

Rienecker, M. M., Suarez, M. J., Gelaro, R., Todling, R., Bacmeister, J., Liu, E., Bosilovich, M. G., Schubert, S. D., Takacs, L., Kim, G.-K., Bloom, S., Chen, J., Collins, D., Conaty, A., da Silva, A., Gu, W., Joiner, J., Koster, R. D., Lucchesi, R., Molod, A., Owens, T., Pawson, S., Pegion, P., Redder, C. R., Reichle, R., Robertson, F. R., Ruddick, A. G., Sienkiewicz, M., and Woollen, J.: MERRA: NASA's Modern-Era Retrospective Analysis for Research and Applications, J. Climate, 24, 3624–3648, doi:10.1175/JCLI-D-11-00015.1, 2011.

Sea-Bird Electronics: SBE 41/41CP CTD Module for Autonomous Profiling Floats (Argo), http://www.seabird.com/sbe41-argo-ctd, accessed 02 Aug 2016, 2016.

Takeshita, Y., Martz, T. R., Johnson, K. S., Plant, J. N., Gilbert, D., Riser, S. C., Neill, C., and Tilbrook, B.: A climatology-based quality control procedure for profiling float oxygen data, J. Geophys. Res.-Oceans, 118, 5640–5650, doi:10.1002/jgrc.20399, 2013.

Tengberg, A., Hovdenes, J., Andersson, H. J., Brocandel, O., Diaz, R., Hebert, D., Arnerich, T., Huber, C., Körtzinger, A., Khripounoff, A., Rey, F., Ronning, C., Schimanski, J., Sommer, S., and Stangelmayer, A.: Evaluation of a lifetime-based optode to measure oxygen in aquatic systems, Limnol. Oceanogr.: Methods, 4, 7–17, doi:10.4319/lom.2006.4.7, 2006.

Testor, P., Mortier, L., Karstensen, J., Mauri, E., Heywood, K. J., Hayes, D., Alenius, P., Alvarez, A., Barrera, C., Beguery, L., Bernardet, K., Bertino, L., Beszczynska-Möller, A., Carval, T., Counillon, F., Dumont, E., Griffiths, G., Haugan, P. M., Kaiser, J., Kasis, D., Krahmann, G., Llinas, O., Merckelbach, L., Mourre, B., Nittis, K., Onken, R., D'Ortenzio, F., Pouliquen, S., Proelß, A., Riethmüller, R., Ruiz, S., Sherwin, T., Smeed, D., Stemmann, L., Tikka, K., and Tintore, J.: EGO : towards a global glider infrastructure for the benefit of marine research and operational oceanography, Mercator Ocean – CORIOLIS Quarterly Newsletter, pp. 12–15, http://archimer.ifremer.fr/doc/00114/22554/, 2012.

Uchida, H., Kawano, T., Kaneko, I., and Fukasawa, M.: In Situ Calibration of Optode-Based Oxygen Sensors, J. Atmos. Oceanic Technol., 25, 2271–2281, doi:10.1175/2008JTECHO549.1, 2008.